Bioconjugate Chemistry

Article

pubs.acs.org/bc

Activatable Cell Penetrating Peptide-Conjugated Nanoparticles with Enhanced Permeability for Site-Specific Targeting Delivery of Anticancer Drug

Huimin Xia,[†,§] Guangzhi Gu,[†] Quanyin Hu,[†] Zhongyang Liu,[†] Mengyin Jiang,[∥] Ting Kang,[†] Deyu Miao,[∥] Qingxiang Song,[‡] Lei Yao,[‡] Yifan Tu,[†] Hongzhuan Chen,[‡] Xiaoling Gao,*[,‡] and Jun Chen*[,†]

[†]Key Laboratory of Smart Drug Delivery, Ministry of Education & PLA, School of Pharmacy, Fudan University, 826 Zhangheng Road, Shanghai, 201203, PR China

[‡]Department of Pharmacology, Institute of Medical Sciences, Shanghai Jiaotong University School of Medicine, 280 South Chongqing Road, Shanghai, 200025, PR China

[§]Shanghai Institute for Food and Drug Control (SIFDC), 1500 Zhangheng Road, Shanghai, 201203, PR China

[∥]School of Pharmacy, Shandong University of Traditional Chinese Medicine, Jinan, Shangdong, 250355, PR China

ABSTRACT: Based on the powerful cell-penetrating ability of low molecular weight protamine (LMWP) and the overexpression of matrix metalloproteinases in the tumor sites, we constructed an activatable low molecular weight protamine (ALMWP) and modified it onto the surface of poly(ethylene glycol)-poly(lactic acid) nanoparticles to develop a "smart" drug delivery system with enhanced permeability for facilitating site-specific targeting delivery of anticancer drug. The obtained ALMWP-functionalized nanoparticles (ALMWP-NP) with a particle size of 134.0 ± 4.59 nm and a zeta potential of −34.4 ± 2.7 mV, exhibited an enhanced MMP-dependent accumulation in HT-1080 cells via both energy-independent direct translocation and clathrin-mediated, cytoskeleton-dependent endocytosis. Pharmacokinetic and biodistribution study in HT-1080 tumor-bearing mice showed that ALMWP-NP significantly increased the accumulation of paclitaxel (PTX) in the tumor site but not the nontarget tissues. In addition, intratumor distribution analysis demonstrated that more ALMWP-NP penetrated deeply into the tumor parenchyma. As a result, PTX loaded by ALMWP-NP exhibited improved antitumor efficacy over that by unmodified nanoparticles and LMWP-functionalized nanoparticles. The findings suggested that ALMWP-NP could be used as a safe and effective tumor-targeting drug delivery system and opened a new gateway to the application of cell-penetrating peptides for targeted antitumor therapy.

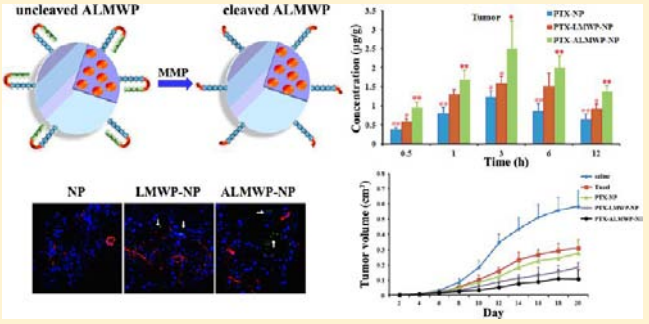

INTRODUCTION

Targeted delivery of therapeutic agents to the tumors is a fundamental approach to cancer therapy. Various strategies have been explored to increase drug delivery into the tumor, among which nanotechnology plays a unique role in the revolutionary development of tumor-targeting drug delivery, imaging, and diagnosis. Upon the administration of nanoscale drugs into the tumor site, the major challenge lies in the design of drug delivery systems (DDS) that can accumulate in the tumor site specifically, get internalized into the tumor cells effectively, and penetrate deeply into the tumor parenchyma.[1]

Nanoparticulate DDS, especially those with stealth properties, can effectively passively target to the tumor sites by taking advantage of the enhanced permeability and retention (EPR) effect.[2] Active targeting based on tumor-specific molecules such as antibodies, peptides, or vitamins that specifically bind to antigens or receptors expressed at high levels in tumor cells or their associated vasculature can help in rendering the accumulation and uptake of nanoparticulate DDS at the tumors sites.[3] However, robust tumor specificity of small molecule ligands for endogenous receptors is rare, and few of these approaches effectively deliver the therapeutics deeply in the tumor parenchyma.[4,5] Therefore, it is of great importance to design functional nanoparticulate DDS with high tumor-targeting efficiency and tumor penetration.

Cell-penetrating peptides (CPPs), composed of multiple positively charged arginine and lysine, show the capability of effectively translocating various cargoes such as protein, nucleic acid, siRNA, antisense peptide nucleic acid (PNA), and polymeric nanoparticles into mammalian cells without requiring specific receptors.[6−9] Among CPPs, low-molecular-weight protamine (LMWP) (CVSRRRRRRGGRRRR) demonstrates remarkable advantages such as being as potent as TAT in mediating cellular translocation of the attached cargos,

Received: September 16, 2012
Revised: January 8, 2013
Published: January 28, 2013

neither antigenic nor mutagenic, and can be produced in mass quantities directly from native protamine.[10−12] More importantly, the amino acid sequence of LMWP fits the C-end Rule (CendR), which has been claimed to be able to specifically target neuropilin-1 protein on tumor cells, be internalized into the cells, induce vascular leakage and tissue penetration, and mediate infiltration into tumor parenchyma.[13] Therefore, LMWP is considered as a promising CPP that can facilitate the intratumor cargo penetration. The issue remained is how to improve its tumor-targeting efficiency and reduce its nonselective accumulation in the nontarget tissues.

A novel strategy termed activatable cell penetrating peptides (ACPP) developed by Tisen's group[14] might represents a promising resolution to the LMWP-mediated drug delivery dilemma. The reported ACCP contain a sequence of polycationic CPP, a polyanionic inhibitory domain and a peptide linker matrix which is sensitive to metalloproteinases (MMP), whose activity is intimately involved in the process of tumor invasion and metastasis.[15] In the MMP-rich tumor environment, the linker is selectively cleaved and the inhibitory acidic peptide dissociates based on its off-rate, thereby exposing the cationic CPP to deliver its linked cargo into the surrounding tumor cells.

Learning from this ACPP strategy, in the present work, we designed and constructed an activatable low molecular weight protamine (ALWMP, E10-PLGLAG-VSRRRRRRGGRRRR) in which the positive charges on the LWMP necessary for transduction were initially masked by a polyanionic peptide (E10) sequence, a MMP-2/9 cleavable peptide linker sequence PLGLAG[16] was utilized as the linker. ALMWP was applied as a novel tumor-targeting ligand and modified to the surface of poly(ethylene glycol)-poly(lactic acid) (PEG-PLA) nanoparticles for enhanced tumor targeting and penetration of the loaded anticancer drugs. This system was expected to possess two superior advantages: First, the overall neutral charge of ALMWP would greatly reduce the recognization of the formulation by the monocyte−macrophage system, retain the stealth properties of the pegylated nanoparticles, reduce their accumulation in the nontargeted organs, and render passive tumor-targeting via the EPR effect; Second, after arriving at the tumor site, the linker would be cleaved by tumor-specific protease MMP-2/9, enabling the exposure of LMWP to mediate a strong intratumor penetration and cellular uptake of the functionalized nanoparticles.

EXPERIMENTAL PROCEDURES

Materials, Cells, and Animals. ALMWP were synthesized by ChinaPeptides Co., Ltd. (Shanghai, China). The copolymers of methoxy poly(ethylene glycol)$_{3000}$-poly(lactic acid)$_{34000}$ (MePEG-PLA) and maleimide-poly (ethylene glycol)$_{3400}$-poly-(lactic acid)$_{34000}$ (Male-PEG-PLA) were kindly provided by East China University of Science and Technology. Paclitaxel (PTX) was purchased from Xi'an Sanjiang Biological Engineering Co. Ltd., and Taxol from Bristol-Myers Squibb Company. Coumarin-6, coumarin-7, DiR (1,1′-dioctadecyl-3,3,3′,3′-tetramethyl indotricarbocyanine iodide), and Triton X-100 were all obtained from Sigma-Aldrich (St. Louis, MO, USA). DAPI (4,6-diamidino-2-phenylindole) was provided by Molecular Probes (Eugene, OR, USA), and cell counting kit-8 (CCK-8) by Dojindo Laboratories (Japan). Dulbecco's Modified Eagle Medium (DMEM) (high glucose) cell culture medium, certified fetal bovine serum (FBS), penicillin/streptomycin stock solutions, and 0.25% Trypsin-EDTA were obtained from Invitrogen Co., USA. Trypan blue was purchased from Beyotime Institute of Biotechnology, goat serum from BOSTER Bio-Engineering Co., Ltd. (Wuhan, China), and CD31 antibody from BioLegend (San Jose, CA, USA). All the other chemicals were of analytical grade and used without further purification.

HT-1080 cell line was obtained from The Cell Bank of Type Culture Collection of Chinese Academy of Sciences, Shanghai Institute of Cell Biology, Chinese Academy of Sciences, and brain capillary endothelial cell bEnd.3 cell line was kindly provided by Prof. Yaocheng Rui, Department of Pharmacology, School of Pharmacy, The Second Military Medical University, Shanghai, PR China.

Adult male BALB/c nude mice (18−20 g) and male Sprague−Dawley rats (180−220 g) were obtained from Experimental Animal Center of Fudan University and maintained at 25 ± 1 °C with free access to food and water. The protocol of animal experiments was approved by the Animal Experimentation Ethics Committee of Fudan University.

Preparation of PTX-Loaded Nanoparticles. PEG-PLA nanoparticles loaded with PTX were prepared using an emulsion/solvent evaporation technique.[17] MePEG-PLA (22.5 mg), Male-PEG-PLA (2.5 mg), and 1% (w/w) of PTX were dissolved in 1 mL dichloromethane, and then added into 2 mL of 1% sodium cholate aqueous solution with the mixture emulsified by sonication (240 w, 2.4 min) on ice using a probe sonicator (Ningbo Scientz Biotechnology Co. Ltd., China). The O/W emulsion was further diluted into a 8 mL of 0.5% sodium cholate aqueous solution under rapid magnetic stirring for 5 min. After evaporating dichloromethane at 30 °C with a ZX-98 rotavapor (Shanghai Institute of Organic Chemistry, China), the obtained nanoparticles were concentrated by centrifugation at 14 000 rpm for 45 min using a TJ-25 centrifuge (Beckman Counter, USA). With the supernatant discarded, the nanoparticles were resuspended in 0.01 M HEPES buffer (pH 7.0) and modified with ALMWP/LMWP via a maleimide−thiol coupling reaction at room temperature for 8 h. The products were then eluted with 0.01 M HEPES buffer (pH 7.0) through a 1.5 × 20 cm Sepharose CL-4B column to remove the unentrapped PTX and unconjugated peptide. Fluorescently labeled nanoparticles were prepared with the same procedure except that 0.1% (w/w) of coumarin-6 or 1% (w/w) of DiR to the copolymer was added for encapsulation.

Characterization of the Nanoparticles. Particle size and zeta potential of the nanoparticles were determined using a Malvern Zeta Sizer Nano series (Malvern Instruments, Worcestershire, UK). Morphological examination was performed via a transmission electron microscope (TEM, H-600, Hitachi, Japan). In order to verify the surface modification of nanoparticle with ALMWP, the samples were lyophilized via an Alpha 2−4 Freeze-Dryer (0.070 Mbar vacuum, −80 °C, Martin Christ, Germany) and subjected to X-ray photoelectron spectroscopy (XPS) analysis.

Drug Encapsulation Efficiency and Loading Capacity. For determining the encapsulation efficiency and loading capacity of PTX-loaded nanoparticles, a predetermined amount of nanoparticles were dissolved in acetonitrile to release PTX. The PTX level was analyzed with an Agilent 1100 HPLC system (Agilent Technologies, CA, USA) using a Dikma Diamonsil C18 column (200 mm × 4.6 mm, 5 μm) with methanol and water (75/25 v/v) as the mobile phase at the flow rate of 1.2 mL/min. The column temperature was

dx.doi.org/10.1021/bc300520t | Bioconjugate Chem. 2013, 24, 419−430

maintained at 40 °C, injection volume was 20 μL, and the detection wavelength was 227 nm. The encapsulation efficiency (%) and loading capacity (%) of the PTX-loaded nanoparticles were calculated using the following equation:

$$\text{encapsulation efficiency}(\%) = \frac{\text{amount of PTX in the nanoparticles}}{\text{total amount of PTX added}} \times 100\%$$

$$\text{loading capacity}(\%) = \frac{\text{amount of PTX in nanoparticles}}{\text{nanoparticle weight}} \times 100\%$$

In Vitro Drug Release. In vitro drug release was performed using an equilibrium dialysis method.[18] Briefly, 1 mL of PTX-loaded nanoparticles (containing 80 μg PTX) was introduced into a dialysis bag (MWCO = 14 000 Da). The bag was then sealed, immediately immersed in 39 mL of release medium (PBS, pH 7.4, with 0.5% Tween-80 to provide sink condition) and incubated at 37 °C at the shaking speed of 100 rpm. At designated time points (1, 2, 3, 4, 6, 8, 12, 24, 48, 72, and 96 h), 0.2 mL of the release sample was withdrawn, and immediately, an equal volume of fresh dissolution medium were replenished. The concentration of PTX in the samples was determined by HPLC as described above.

Cell Culture. HT-1080 cells, human fibrosarcoma cell line, with expression of both MMP-2 and MMP-9,[14,19,20] and bEnd.3 cells, immortalized mouse brain endothelial cell line were maintained in Dulbecco's Modified Eagle Medium (DMEM) supplemented with 10% FBS, penicillin (100 U/mL), and streptomycin (100 μg/mL) under standardized conditions (95% relative humidity, 5% CO_2, 37 °C).

Cellular Association and Uptake of the Nanoparticles. Using coumarin-6 as the fluorescence probe, cellular association of the nanoparticles was evaluated as described previously.[21] Briefly, HT-1080 cells were seeded in a 96-well plate at the density of 5×10^3 cells/well. Twenty-four hours later, the cells were incubated with coumarin-6-loaded unmodified nanoparticles (NP), LMWP-modified nanoparticles (LMWP-NP), and ALMWP-modified nanoparticles (ALMWP-NP) (100−600 μg/mL nanoparticles in HBSS) for 30 min at 37 °C. At the end of the experiment, the cells were washed three times with PBS and fixed with 3.7% formaldehyde for 10 min. After that, the cells were washed three more times with PBS, and observed under a fluorescent microscope (Olympus, Japan).

Quantitative analysis of cellular association of coumarin-6-loaded NP, LMWP-NP, and ALMWP-NP was conducted using a high content analysis system.[22] HT-1080 cells were plated on a 96-well plate at the density of 5×10^3 cells/well. Twenty-four hours later, the cells were incubated with the nanoparticles (50−600 μg/mL) for 30 min at 4 and 37 °C, respectively. To determine if the cellular association of the nanoparticles was time dependent, the cells were incubated with the nanoparticles (200 μg/mL) at 37 °C for 15, 30, and 60 min, respectively. For determining the level of cellular internalized nanoparticles, the cells were incubated with Trypan blue (Beyotime Institute of Biotechnology) to quench those fluorescent signals from the uninternalized ones, and subjected to a second high content analysis system analysis.[23]

In order to reveal the mechanism of cellular interaction of ALMWP-NP in HT-1080 cells, cellular association and uptake of the nanoparticles were determined in the presence of various endocytosis inhibitors. The cells were preincubated for 30 min with 500 ng/mL LMWP, 500 ng/mL ALMWP, 10 μg/mL chlorpromazine, 4 μg/mL colchicines, 10 μg/mL Cytochalasin D (Cyto-D), 5 μg/mL Brefeldin A (BFA), 5 μg/mL filipin, 10 mM NaN_3, 50 mM deoxyglucose, 2.5 mM methyl-β-cyclodextrin (M-β-CD), 200 nM monensin, and 20 μM nocodazole, respectively, and then incubated with 90 μg/mL of NP/LMWP-NP/ALMWP-NP at 37 °C for 30 min. After that, quantitative analysis was performed as described above.

MMP-specific inhibitor, metastat,[24] was used to determine if the cellular uptake of ALMWP-NP is a MMP-dependent process. After preincubated with metastat (1 μM) for 30 min, cellular uptake of ALMWP-NP in HT-1080 cells was quantitative determined as mentioned above and compared with that of the noninhibited control. In addition, cellular uptake of ALMWP-NP was also evaluated in bEnd.3 cells with negligible expression of MMP-2/9 in both the absence and presence of metastat.

In Vitro Cytotoxicity of the Nanoparticles. To evaluate the safety of the nanoparticles (NP, LMWP-NP, and ALMWP-NP) to normal cells, bEnd.3 cells with negligible expression of MMP-2/9, and showing no significant difference in the cellular uptake of the three kinds of nanoparticles, were utilized as the cell model. The cells were seeded into 96-well plates at the density of 5×10^3 cells/well and incubated at 37 °C, 5% CO_2, for 24 h to allow cell attachment. After that, the cells were incubated with NP, LMWP-NP, and ALMWP-NP (0.01−8.0 mg/mL in the culture media), respectively, at 37 °C for 4 h. Following the treatment, cell viability was measured by a CCK-8 assay according to the manufacturer's instruction. Cell viability was expressed as the percentage of absorbance in comparison with that of the control (cells treated with the culture medium only).

In Vivo Imaging of NP, LMWP-NP, and ALMWP-NP. Biodistribution and tumor targeting efficiency of ALMWP-NP was evaluated in nude mice bearing HT-1080 human fibrosarcoma xenografts using near-infrared dye DiR as the fluorescent probe as described previously.[22] The animal model was established by injecting HT-1080 cells (1×10^7 cells suspended in 0.15 mL of cell culture medium) subcutaneously in the right flank of the mouse. Under anesthesia, the animals were intravenously injected with the nanoparticles (0.5 mg DiR/kg, $n = 3$) via the tail vein. Fluorescent image of each mouse was captured at selected time points post administration. Eight hours after administration, the animals were euthanized and heart perfused with 100 mL of saline, with the tumors, hearts, livers, spleens, lungs, and kidneys harvested and subjected to imaging under a Maestro in vivo imaging system (CRI, MA).

Tumor Permeability Analysis. In order to study the tumor permeability profile of ALMWP-NP, coumarin-6-labeled NP, LMWP-NP, and ALMWP-NP were given to three groups of nude mice harboring HT-1080 human fibrosarcoma xenografts ($n = 3$) via tail vein injection. Each animal received a total amount of nanoparticles containing coumarin-6 20 μg in 200 μL. Three hours later, after heart perfusion with saline and 4% paraformaldehyde, the tumors were removed, fixed in 4% paraformaldehyde for 24 h, dehydrated in sucrose solution, and subjected to OCT (Sakura, Torrance, CA, USA) embedding and frozen section. After that, the slides were stained by immunofluorescence with anti-CD31 to show the tumor vasculature: the frozen slices were treated with a permeabilization buffer (0.2% Triton/PBS solution) for 5 min, blocked with

dx.doi.org/10.1021/bc300520t | Bioconjugate Chem. 2013, 24, 419−430

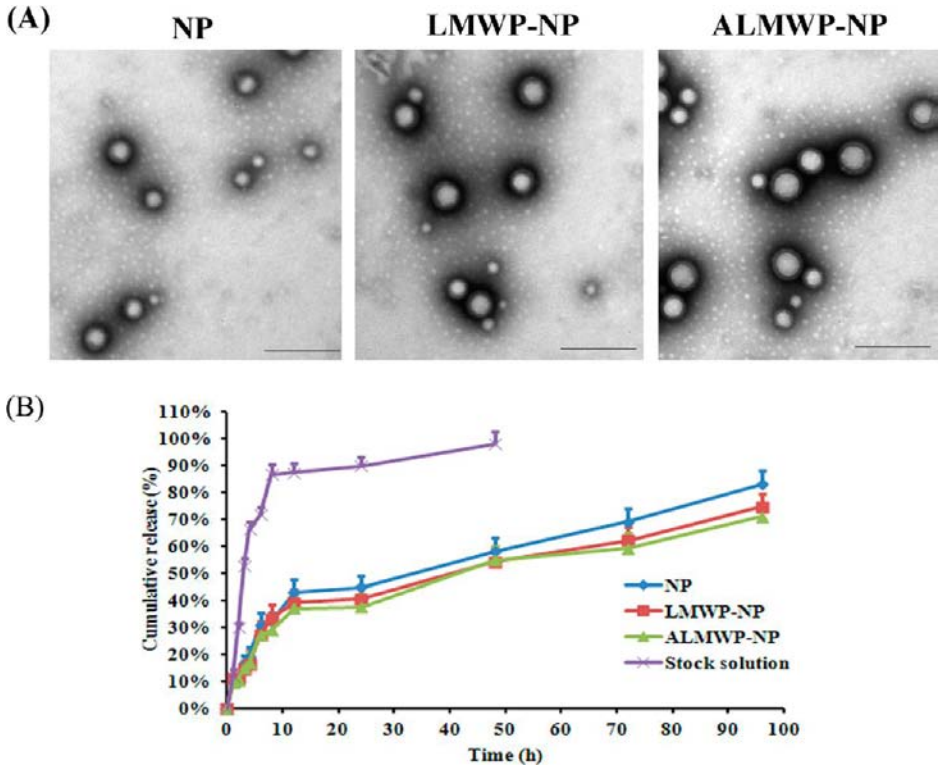

Figure 1. (A) Transmission electron micrograph of NP, LMWP-NP, and ALMWP-NP negatively stained with phosphotungstic acid solution. Bar, 200 nm. (B) Release profiles of PTX from stock solution, PTX-NP, PTX-LMWP-NP, and PTX-ALMWP-NP in pH 7.4 PBS (containing 0.5% Tween 80) (n = 3, mean ± SD).

20% goat serum for 60 min, incubated overnight at 4 °C with the Alexa Fluor 647-conjugated antimouse CD31 antibody (1:100), rinsed three times with PBS, and then stained with DAPI for 8 min. Finally, the slices were rinsed three times with PBS, sealed with glycerophosphate, and subjected to confocal microscopy analysis under a Zeiss LSM 510 microscope.

Pharmacokinetic Study. SD rats were randomly divided into four groups (n = 3) and intravenously administrated via the tail vein with Taxol, PTX-loaded NP (PTX-NP), PTX-loaded LMWP-NP (PTX-LMWP-NP), and PTX-loaded ALMWP-NP (PTX-ALMWP-NP), respectively, at the dose of 5 mg/kg PTX. Blood was collected in the tube with heparin at 0.083, 0.25, 0.5, 1, 2, 3, 4, 6, 8, 12, and 24 h after intravenous administration. The plasma was collected following centrifugation at 3000 rpm for 10 min and stored at −20 °C until assays.

Biodistribution and tumor targeting efficiency of PTX-ALMWP-NP were also quantitatively evaluated on nude mice bearing HT-1080 human fibrosarcoma xenografts, and compared with that of PTX-NP and PTX-LMWP-NP. The mice were randomly divided into three groups (n = 3) and intravenously administered with PTX-NP, PTX-LMWP-NP, and PTX-ALMWP-NP at the dose of 5 mg/kg PTX, respectively. At predetermined time points (0.5, 1, 3, 6, and 12 h) following administration, the animals were sacrificed with the heart, liver, spleen, lung, kidney, and tumor collected and stored at −20 °C until analysis.

Tissue samples for analysis were homogenized with 3-fold volumes of distilled water and subjected to protein precipitation as described previously using docetaxel as the internal standard.[25] The plasma samples were treated in the same manner without the addition of water. An API 4000 triple quadrupole liquid chromatography−tandem mass spectrometry (LC-MS/MS) analysis system (Applied Biosystems, Toronto, Canada) was used for determining the level of PTX.[18] Detection of the ions was performed in the multiple-reaction monitoring (MRM) mode, by monitoring the transition pairs of m/z 876.4 precursor ion to the m/z 308.1 for PTX and m/z 830.2 precursor ion to the m/z 549.3 for docetaxel. Drug and Statistics software for Windows (*DAS* v 2.1.1) was used for the calculation of the pharmacokinetic parameters.

Antiproliferation Assay. HT-1080 cells were seeded in 96-well plates at the density of 5×10^3 cells/well. Twenty-four hours later, the cells were incubated with Taxol, PTX-NP, PTX-LMWP-NP, and PTX-ALMWP-NP, respectively at the PTX concentrations of 0−40 μg/mL for 48 h (n = 3). After treatment, cell viability was evaluated with the CCK-8 assay as mentioned above. GraphPad *Prism* v 5.0 was used for IC_{50} calculation.

In Vivo Antitumor Activity. Nude mice animal model bearing HT-1080 human fibrosarcoma xenografts was established as described above and used for evaluating the in vivo antitumor activity of the formulations. Six days after the implantation, the mice were randomly divided into five groups (n = 6) and intravenously administered via the tail vein with Taxol, PTX-NP, PTX-LMWP-NP, PTX-ALMWP-NP, and saline, respectively, at the dose of 5 mg/kg PTX. The treatment was repeated every three days for five consecutive injections. The tumor size was measured every other day with a vernier caliper in two dimensions until the 20th day on which the animals were sacrificed. Individual tumor volume (V) was calculated using the formula $V = 2\pi \times dl \times ds/6$, wherein dl represents the longest diameter and ds represents the shortest diameter. At the end of the experiment, the animals were sacrificed with the tumor harvested and weighed. The

dx.doi.org/10.1021/bc300520t | *Bioconjugate Chem.* 2013, 24, 419−430

inhibitory rate was calculated with the formula: $(1 - W_{PTX}/W_{saline}) \times 100\%$, in which W_{PTX} represented the tumor weight of the PTX-treated animals and W_{saline} that of the saline-treated control.

For safety evaluation, body weight of each mouse was determined on alternate days during the experimental period.

Statistical Analysis. All the data were expressed as mean ± standard deviation. Comparison among multiple groups was carried out by one-way ANOVA followed by Bonferroni tests, and statistical significance was defined as $p < 0.05$.

RESULTS

Preparation and Characterization of the Nanoparticles. Representative transmission electron micrographs illustrated that NP, LMWP-NP, and ALMWP-NP were generally spherical with a uniform distribution (Figure 1A). Dynamic light scattering analysis showed that ALMWP-NP and LMWP-NP present slightly bigger particle size than NP. In contrast, in the case of zeta potential, ALMWP-NP exhibit a negative zeta potential (−34.4 mV), which was similar to that of NP (−40.2 mV), while LMWP-NP exhibit a positive one (18.9 mV) (Table 1). XPS analysis showed that the elemental composition percentages of nitrogen on the surface of unconjugated NPs and in the mixed copolymers (22.5 mg MePEG-PLA and 2.5 mg Male-PEG-PLA) were undetectable, while that on the surface of ALMWP-NP was 1.31%.

Table 1. Particle Size and Zeta Potential of PTX-Loaded Nanoparticles

PTX-loaded nanoparticles	mean size (mean ± SD, nm)	zeta potential (mV)
PTX-NP	118.8 ± 2.17	−40.2 ± 2.1
PTX-LMWP-NP	134.4 ± 12.11	18.9 ± 1.8
PTX-ALMWP-NP	134.0 ± 4.59	−34.4 ± 2.7

Drug Encapsulation Efficiency and Loading Capacity. Encapsulation efficiency of the optimized PTX-loaded NP, LMWP-NP, and ALMWP-NP was 41.9 ± 2.01%, 46.3 ± 3.14%, and 41.8 ± 2.33%, respectively, at the loading capacity of 0.82 ± 0.06%, 0.97 ± 0.07%, and 0.86 ± 0.064%, respectively (n = 3).

In Vitro Drug Release. As shown in Figure 1B, the release of PTX from the stock solution was quick (about 90% in 4 h). In contrast, a similar sustained biphasic drug release, which was composed of a relative fast drug release in first 24 h (40% release) and a slower one in the following 72 h (30% release), was obtained for all the PTX-loaded nanoparticles (NP, LMWP-NP, and ALMWP-NP).

Fluorescent Microscopy Analysis. Fluorescent microscopy analysis showed that after 30 min exposure to coumarin-6-loaded NP, LMWP-NP, and ALMWP-NP, the enhancement of cellular associated fluorescence correlated well with the increase of nanoparticle concentration (Figure 2). Apparently higher accumulation of the fluorescent signal was observed in those cells treated with coumarin-6-loaded ALMWP-NP than that with NP, and also slightly higher than that with LMWP-NP especially at high concentrations.

High Content Analysis System Analysis. Quantitative high content analysis system analysis showed a concentration-, time-, and temperature-dependent cellular association of ALMWP-NP in HT-1080 cells (Figure 3A,B,C). At each time and concentration point, cellular association of ALMWP-NP was higher than that of NP (about 7.47 times higher than that of NP after 30 min incubation at the concentration of 400 μg/mL), and similar to or slightly higher than that of LMWP-NP especially at high concentrations. By quenching the fluorescent signal of the uninternalized nanoparticles with Trypan blue, cellular uptake of ALMWP-NP was found to be much higher than that of NP (about 30.92 times higher than that of NP after 30 min incubation at the concentration of 400 μg/mL) (Figure 3E), and similar to or slightly higher than that of LMWP-NP especially at high concentrations. In addition, cellular association of ALMWP-NP at 4 °C is still high, even higher than that of NP at 37 °C (Figure 3A,D).

Mechanism of Cellular Interaction of the Nanoparticles. Endocytosis inhibition experiments were performed to investigate the mechanism of cellular interaction with the nanoparticles. It was shown that cellular association of LMWP-NP was inhibited by chlorpromazine and cyto-D (Figure 4C), and that of ALMWP-NP by chlorpromazine and nocodazole

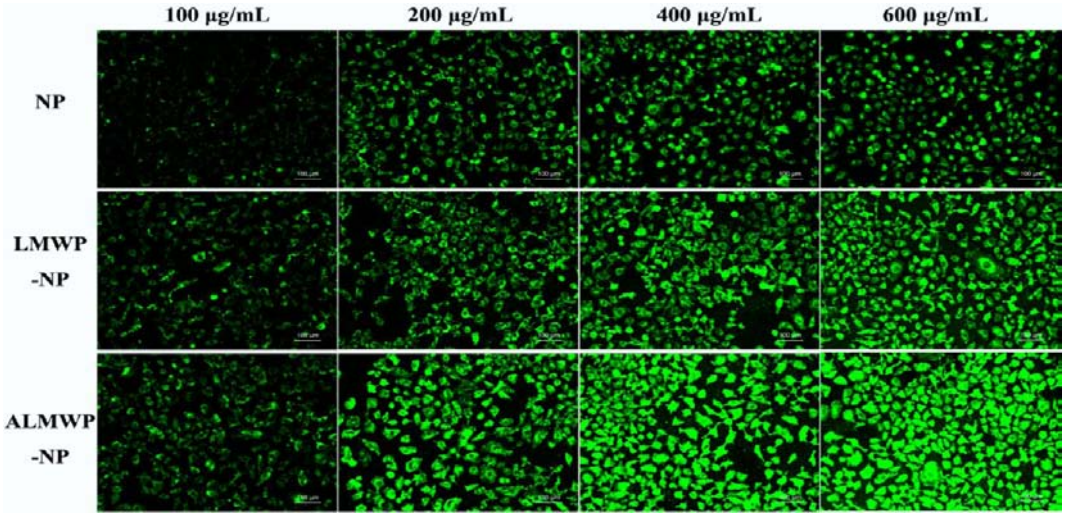

Figure 2. Cellular association of the nanoparticles after 30 min incubation at different concentrations: 100 μg/mL, 200 μg/mL, 400 μg/mL, and 600 μg/mL, respectively.

dx.doi.org/10.1021/bc300520t | Bioconjugate Chem. 2013, 24, 419−430

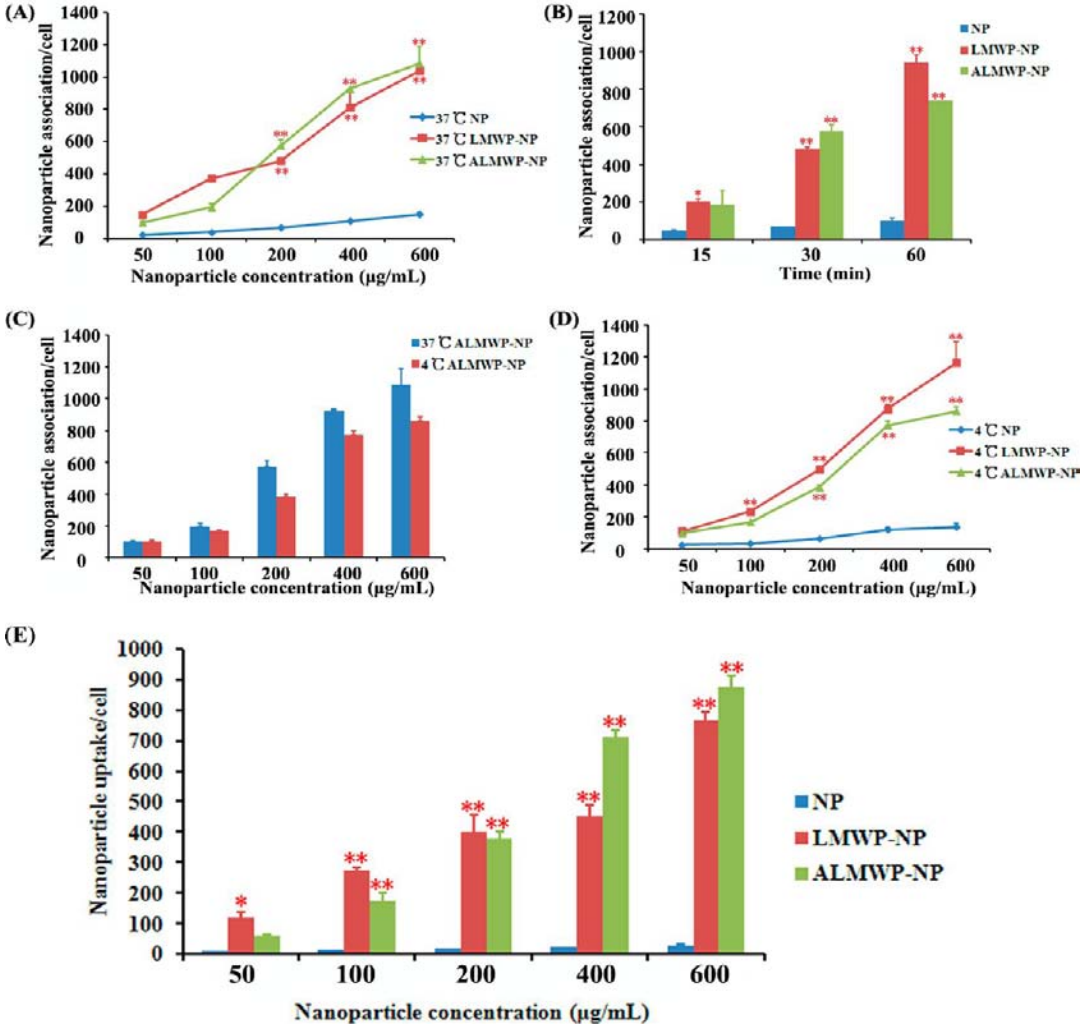

Figure 3. Cellular association and uptake of the nanoparticles in HT-1080 cells. (A) Cellular association of the nanoparticles after 30 min of incubation at nanoparticle concentration from 50 to 600 μg/mL at 37 °C. (B) Cellular association of the nanoparticles after the incubation with 200 μg/mL of nanoparticles at 37 °C for 15, 30, and 60 min, respectively. (C) Cellular association of the nanoparticles after 30 min of incubation with 50−600 μg/mL of ALMWP-NP at 37 and 4 °C, respectively. (D) Cellular association of the nanoparticles after 30 min of incubation at the nanoparticles concentration from 50 to 600 μg/mL at 4 °C. (E) Cellular uptake of NP, LMWP-NP, and ALMWP-NP after 30 min incubation at 37 °C at different concentrations: 50, 100, 200, 400, and 600 μg/mL, respectively. *$p < 0.05$, **$p < 0.01$ significantly different from that of NP at the same temperature, concentration, and incubation time.

(Figure 4B). In contrast, cellular association of NP was reduced in the presence of the inhibitor of lipid raft-mediated endocytosis—M-β-CD. Both LMWP and ALMWP were found to inhibit the cellular association of both LMWP-NP and ALWMP-NP. In addition, the cellular uptake of ALMWP-NP was significantly reduced in the presence of MMP inhibitor, metastat, while that of LMWP-NP was not (Figure 4D). In contrast, in bEnd.3 cells with negligible MMP expression, cellular uptake of ALMWP-NP was significantly lower than that of LMWP-NP, but did not change in the presence of MMP inhibitor (Figure 5).

In Vitro Cytotoxicity. bEnd.3 cells was also used to evaluate the safety of NP, LMWP-NP, and ALMWP-NP to normal cells. After the treatments with both NP and ALMWP-NP up to 4 mg/mL for 4 h, the cell viability was over 90% without significant difference observed between the two groups. In contrast, cell viability was found significantly reduced following the LMWP-NP treatment (Figure 6).

Qualitative in Vivo Imaging. In vivo imaging analysis showed that an obviously stronger fluorescent signal of DiR was detected in the tumor site of those animals administered with DiR-loaded ALMWP-NP when compared with that in those treated with DiR-loaded NP. In contrast, in those animals treated with DiR-loaded LMWP-NP, although improved fluorescence intensity was observed in the tumors, enhanced fluorescence intensity was also observed in the lung and liver (Figure 7).

Tumor Permeability Analysis. Confocal microscopy examination revealed that the fluorescence signal observed in the tumor of those animals treated with ALMWP-NP was much higher than that in LMWP-NP-treated ones, while that of those following NP treatment was almost invisible (Figure 8).

Pharmacokinetic Study. Following intravenous administration in SD rats, PTX-NP and PTX-ALMWP-NP exhibited similar concentration−time profiles with similar C_{max}, AUC_{0-t}, $t_{1/2}$, and CL obtained, while PTX-LMWP-NP showed a faster systemic clearance and lower AUC_{0-t} and Taxol cleared most quickly (Figure 9, Table 2).

Biodistribution. Biodistribution of PTX following intravenous administration of PTX-loaded nanoparticles was

dx.doi.org/10.1021/bc300520t | *Bioconjugate Chem.* 2013, 24, 419−430

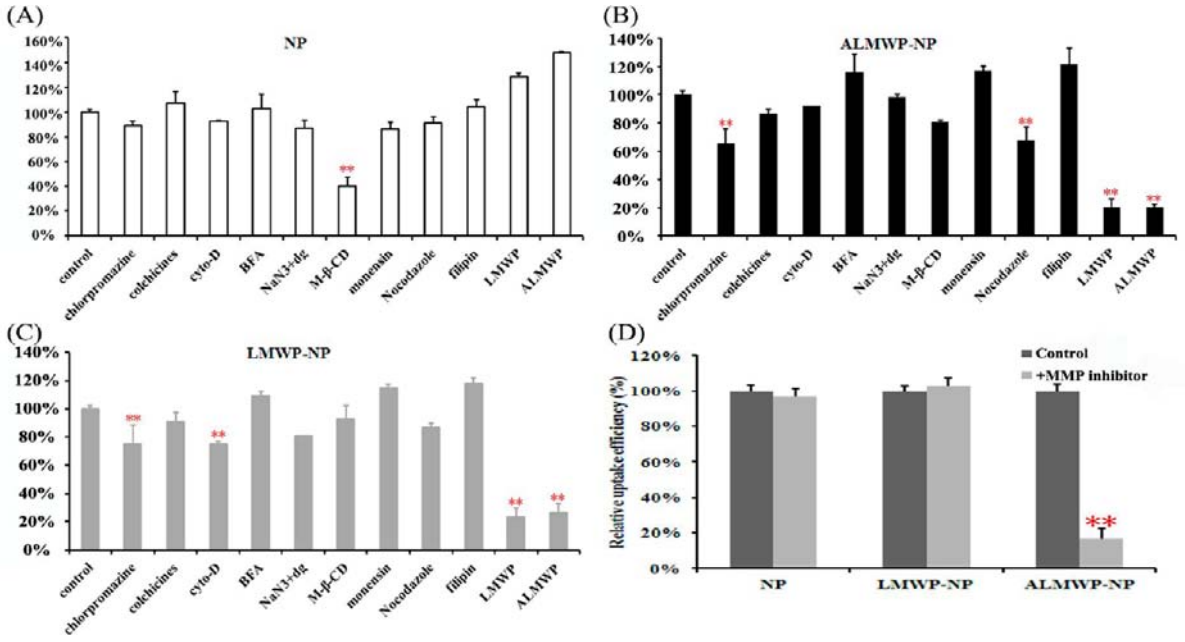

Figure 4. Relative cellular association of nanoparticles in HT-1080 cells in the presence of different endocytosis inhibitors (500 ng/mL LMWP, 500 ng/mL ALMWP, 10 μg/mL chlorpromazine, 4 μg/mL colchicines, 10 μg/mL Cytochalasin D (Cyto-D), 5 μg/mL Brefeldin A (BFA), 5 μg/mL filipin, 10 mM NaN_3, 50 mM deoxyglucose, 2.5 mM methyl-β-cyclodextrin (M-β-CD), 200 nM monensin, and 20 μM nocodazole, respectively): (A) NP; (B) ALMWP-NP; (C) LMWP-NP. (D) Cellular uptake of the nanoparticles in the presence of MMP inhibitor (incubation for 30 min). *p < 0.05, **p < 0.01 significantly different from that of the noninhibitor control.

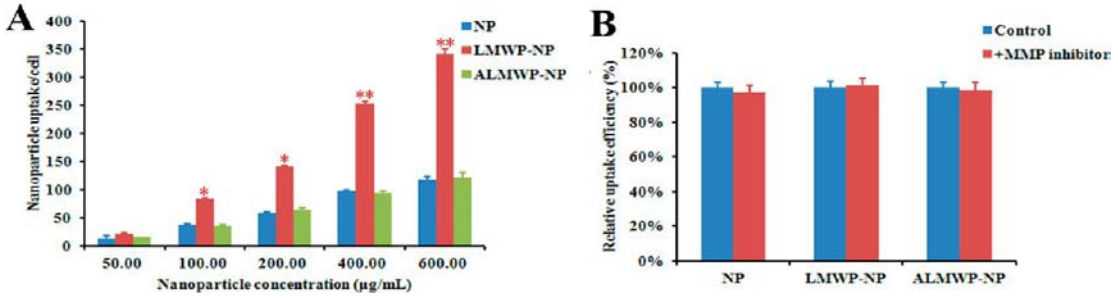

Figure 5. Cellular uptake of the nanoparticles in bEnd.3 cells. (A) Cellular uptake of the nanoparticles after 30 min of incubation at nanoparticle concentration from 50 to 600 μg/mL at 37 °C. (B) Cellular uptake of the nanoparticles in the presence of MMP inhibitor (incubation for 30 min). *p < 0.05, **p < 0.01 significantly different from that of the noninhibitor control.

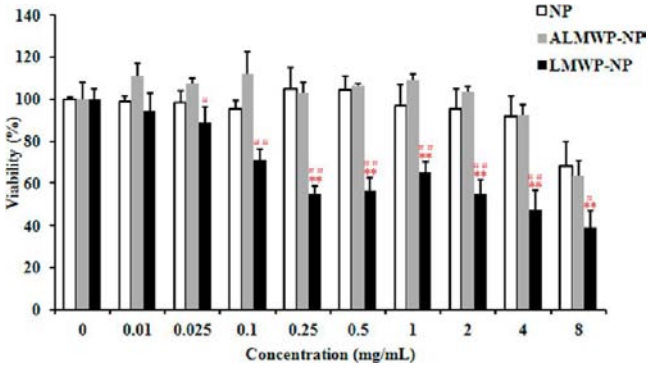

Figure 6. In vitro cytotoxicity of the nanoparticles on bEnd.3 cells at the nanoparticle concentrations ranging from 0 to 8 mg/mL (n = 3). *p < 0.05, **p < 0.01, significantly different from that of negative control (cells treated with the culture medium only); p < 0.05, $^{\#\#}p$ < 0.01, significantly different from that of NP.

assessed in nude mice bearing HT-1080 human fibrosarcoma xenografts. At all time points, PTX concentrations detected in the tumors of those animals receiving the three formulations followed the order: PTX-ALMWP-NP > PTX-LMWP-NP > PTX-NP. Besides, PTX loaded by LWMP-NP was found to exhibit higher accumulation in the liver, spleen, and lung than that of PTX associated to the unmodified NP and ALMWP-NP (Figure 10).

Antiproliferation Assay. The effect of Taxol, PTX-NP, PTX-LMWP-NP, and PTX-ALMWP-NP on tumor cell viability was evaluated by a CCK-8 assay. Apparent growth suppression on HT-1080 cells was observed after treatment with PTX at the concentrations 0–40 μg/mL. As showed by IC_{50} (the value of IC_{50} for Taxol, PTX-NP, PTX-LMWP-NP, and PTX-ALMWP-NP was 5.540, 6.354, 0.8715, and 1.137 μg/mL, respectively), which was defined as the drug concentration at which 50% cells were inhibited in growth or survival, antiproliferation activity of the formulations followed the order: PTX-LMWP-NP > PTX-ALMWP-NP > Taxol > PTX-NP.

In Vivo Antitumor Activity. In vivo antitumor efficiency of Taxol, PTX-NP, PTX-LMWP-NP, and PTX-ALMWP-NP was evaluated in the tumor-bearing nude mice. No body weight loss

dx.doi.org/10.1021/bc300520t | Bioconjugate Chem. 2013, 24, 419–430

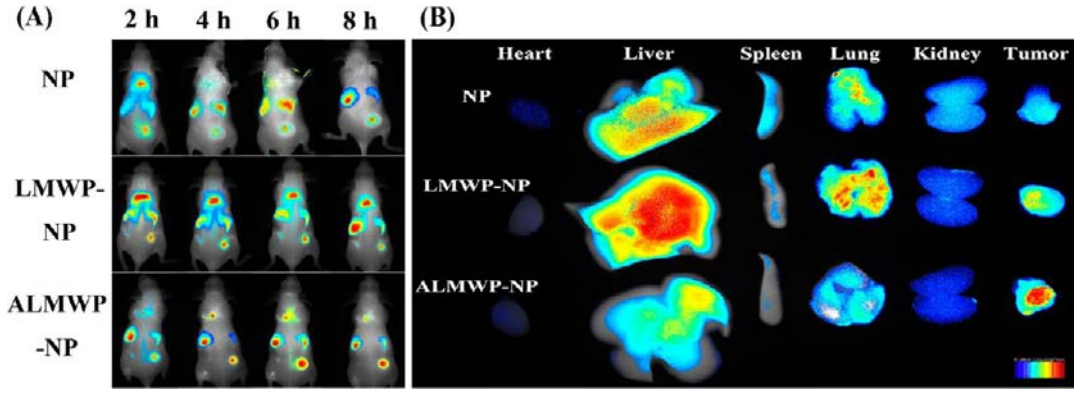

Figure 7. In vivo distribution of DiR-loaded NP, LMWP-NP, and ALMWP-NP at various time points following intravenous administration: (A) in living nude mice; (B) in main organs 8 h after administration.

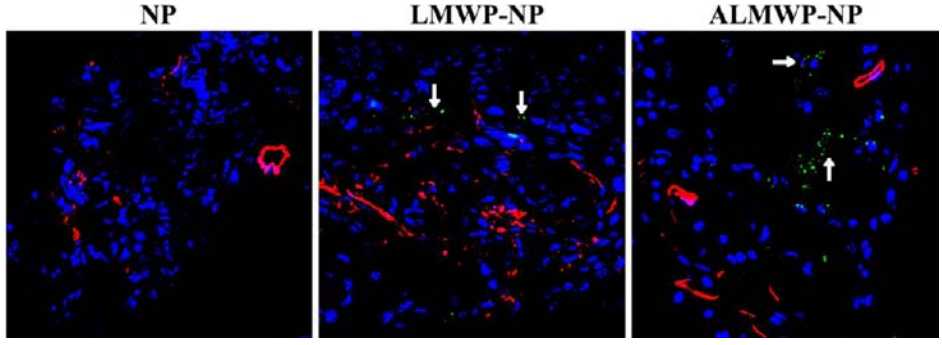

Figure 8. Intratumor distribution of coumarin-6-loaded NP, LMWP-NP, and ALMWP-NP examined under confocal microscopy: red, blood vessels stained with an anti-CD31; green, coumarin-6-loaded nanoparticles; blue, cell nuclei stained with DAPI.

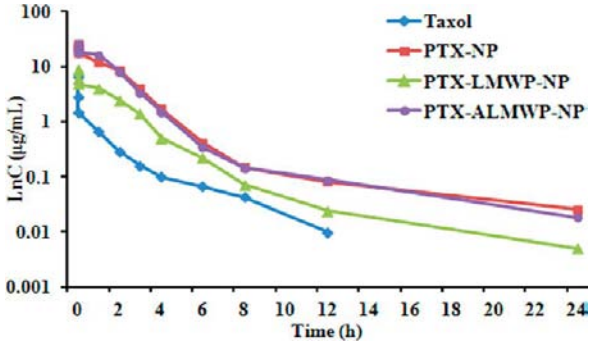

Figure 9. Plasma concentration−time profiles of PTX (μg/mL) after i.v. of Taxol and the PTX-loaded NP (PTX-NP), PTX-loaded LMWP-NP (PTX-LMWP-NP), and PTX-loaded ALMWP-NP (PTX-ALMWP-NP) in SD rats at the PTX dose of 5 mg/kg (mean ± SD, $n = 3$).

was observed in all the PTX treatment groups and that of those nanoparticle-treated animals even slightly increased (Figure 11A). All PTX formulations were effective in preventing tumor growth when compared with saline, and PTX-ALMWP-NP demonstrated the highest inhibitory effect on tumor growth among all the treatment groups ($P < 0.05$) (the tumor inhibition rate for Taxol, PTX-NP, PTX-LMWP-NP, and PTX-ALMWP-NP was 30.53%, 43.02%, 60.95%, and 72.72%, respectively) (Figure 11B,C,D).

DISCUSSION

Protease-activated strategy for tumor site-specific delivery has shown great promise in cancer imaging and therapy.[26−29] Activatable cell-penetrating peptides (ACPPs) represent a new class of promising agents with high permeability that can be activated by specific enzymes in the tumor site. The cell-penetrating function of the polycationic peptide is efficiently blocked by intramolecular electrostatic interactions with a polyanionic peptide. Proteolysis of the cleavable linker between

Table 2. Pharmacokinetic Parameters of PTX after an Intravenous Administration of Taxol, PTX-NP, PTX-LMWP-NP, and PTX-ALMWP-NP, respectively, at the PTX Dose of 5 mg/kg

	Taxol		PTX-NP		PTX-LMWP-NP		PTX-ALMWP-NP	
PK parameters	mean	SD	mean	SD	mean	SD	mean	SD
$AUC_{0\text{-}t}$ (μg/mL·h)	3.64[b]	0.35	41.38	3.01	13.07[b]	0.80	42.79	5.72
$t_{1/2}$ (h)	2.74[a]	0.89	4.63	2.95	3.13[a]	1.46	5.09	0.25
CL (L/h/kg)	1.36[b]	0.12	0.12	0.01	0.38[b]	0.02	0.12	0.01
C_{max} (mg/L)	6.43[b]	0.70	25.27	2.17	9.03[b]	0.79	24.90	2.69

[a] $p < 0.05$. [b] $p < 0.01$, significantly different with that of PTX-ALMWP-NP.

dx.doi.org/10.1021/bc300520t | Bioconjugate Chem. 2013, 24, 419−430

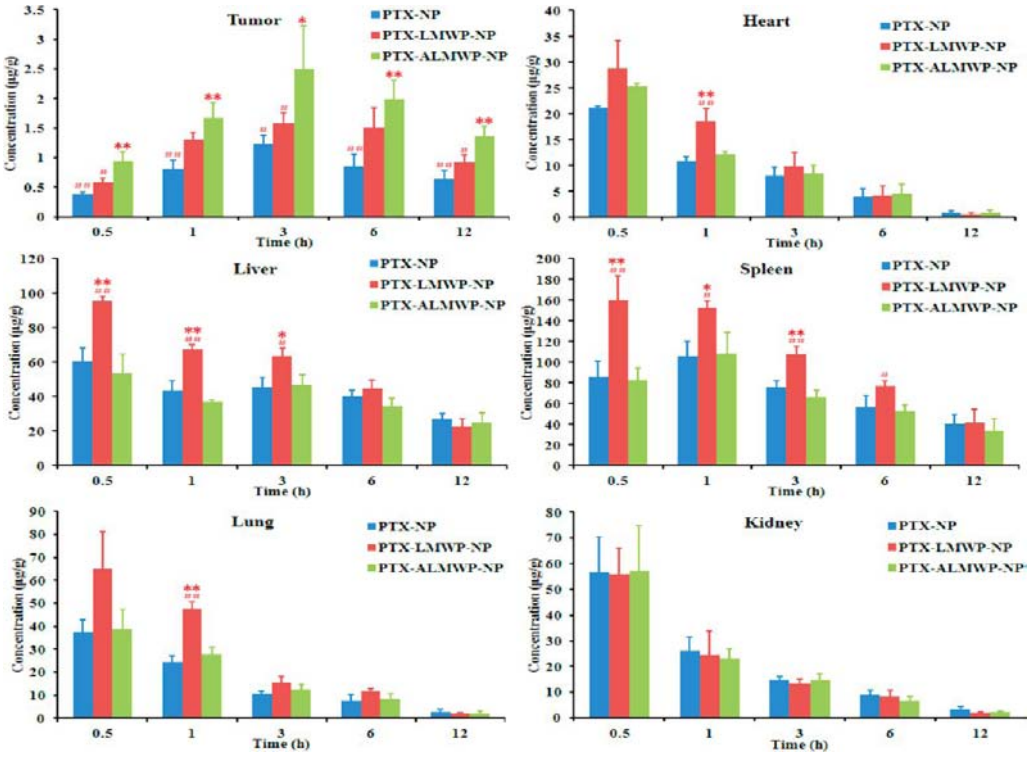

Figure 10. Biodistribution of PTX following intravenous administration of PTX-loaded NP (PTX-NP), PTX-loaded LMWP-NP (PTX-LMWP-NP), and PTX-loaded ALMWP-NP (PTX-ALMWP-NP), respectively, at the PTX dose of 5 mg/kg. $n = 3$. $^{*}p < 0.05$, $^{**}p < 0.01$, significantly different from that of PTX-NP; $^{\#}p < 0.05$, $^{\#\#}p < 0.01$, significantly different from that of PTX-ALMWP-NP.

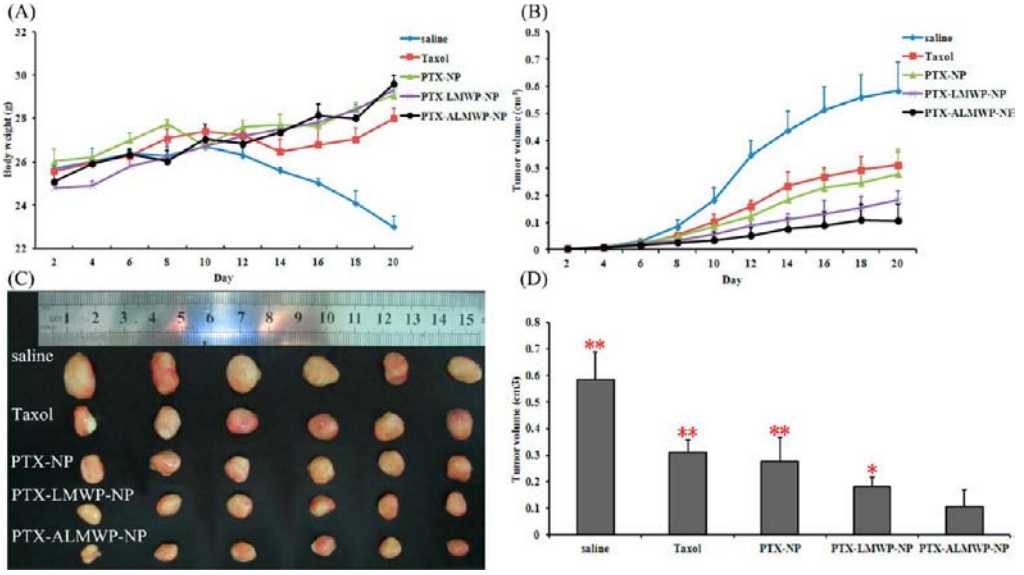

Figure 11. In vivo antitumor activity of Taxol, PTX-loaded NP (PTX-NP), PTX-loaded LMWP-NP (PTX-LMWP-NP), and PTX-loaded ALMWP-NP (PTX-ALMWP-NP) and saline, respectively, after five consecutive injections (repeated every three days) at the dose of 5 mg/kg PTX. (A) Change in body weight of the nude mice harboring HT-1080 tumors during the 20-day experimental period. (B) Tumor growth during the 20-day experimental period. (C) Tumor morphology and size at the experimental end point (20th day). (D) Tumor volume at the experimental end point (20th day). Data represents mean ± SD, $n = 6$. $^{*}p < 0.05$, $^{**}p < 0.01$, significantly different from that of the PTX-ALMWP-NP group.

the polycationic cell-penetrating peptide and polyanionic peptide affords dissociation of the two domains and enables the activated cell-penetrating peptide to mediate effective penetration under specific environment. On the basis of this concept, activatable LMWP (ALMWP) was designed here as a novel ligand to facilitate tumor targeting and penetration of nanoparticulate DDS.

The ALMWP was composed of three domains: a polycationic cell-penetrating peptide (LMWP), a cleavable linker (PLGLAG), which can be cleaved by matrix metalloproteinase (MMP) that specifically expressed on the tumor cell surface, and a polyanionic domain (E10). Nanoparticulate DDS was conjugated to the end of LWMP. The overall surface charge of the constructed ALMWP-NP remained neutral

dx.doi.org/10.1021/bc300520t | *Bioconjugate Chem.* 2013, 24, 419−430

because of the electrostatic interaction between LMWP and E10, which could greatly reduce the clearance of the DDS by the monocyte−macrophage system and also largely decrease its accumulation in the nontargeted tissues. After circulating to the tumor site, the linker sequence would be cleaved by MMP that highly expressed in the tumor, enabling the activation of LMWP to mediate intratumor penetration and cellular uptake of the nanoparticles. Therefore, ALMWP-NP might be practically employed as an attractive and effective nanocarrier for tumor-targeting drug delivery.

ALMWP-NP was here prepared via a maleimide-mediated covalent binding procedure. The obtained ALMWP-NP with an average particle size of 134.0 ± 4.59 nm was expected to present a favorable EPR effect.[30] Due to the electrostatic interaction between LMWP and E10, ALMWP-NP showed a similar negative zeta potential as that of NP. In contrast, LMWP-NP exhibited a positive zeta potential.

In vitro release experiments showed that about 90% release was achieved for PTX solution in 4 h, indicating that PTX can freely diffuse through the dialysis bag, and the dialysis method can be used for studying PTX release from the nanoparticles. PTX release from the three nanoparticles underwent a biphasic release pattern. The burst release of PTX in the first 12 h was believed to be contributed by the agent that was poorly entrapped and located at the periphery of PLA matrix, while the sustained release in the following days was mainly attributed to the diffusion of drug that was well encapsulated and localized in the core of the nanoparticles. Although no significant differences were detected at all time points, the cumulative PTX release from PTX-NP was slightly higher than that from PTX-LMWP-NP and PTX-ALMWP-NP, which we believed was due to the larger size and thus smaller surface of functionalized nanoparticles following LMWP and ALMWP conjugation.

Cellular interaction results showed that ALMWP-NP exhibited a significantly higher cellular association and uptake than NP, and also presented a slightly higher cellular uptake than LMWP-NP at high concentrations (400−600 μg/mL). This could have mainly resulted from the aggregation of LMWP-NP at the high concentrations that hindered its cellular uptake. A time-, temperature-, and concentration-dependent cellular association of ALMWP-NP was observed, suggesting a process of active endocytosis.

To characterize the endocytosis pathways that were involved in the cellular interaction of ALMWP-NP, cellular association and uptake experiments were performed in the presence of various endocytosis inhibitors. Cellular association of both LMWP-NP and ALMWP-NP were inhibited by clathrin and cytoskeleton-dependent pathway inhibitors, suggesting the participation of clathrin-mediated and cytoskeleton-dependent endocytosis in the cellular uptake of LMWP-NP and ALMWP-NP. In addition, cellular internalization of ALMWP-NP was also observed at 4 °C, although lower than that at 37 °C, but still much higher than that of NP at both 37 and 4 °C, suggesting that, besides endocytosis, energy-independent internalization might also be involved in the cellular internalization of ALMWP-NP. As shown in Figure 3, the cellular association of ALMWP-NP is similar to or slightly higher than that of LMWP-NP at 37 °C, but lower at 4 °C, suggesting that the cleavage of ALMWP could be an energy-dependent process. In order to justify the role of MMP in the tumor cell specific internalization of ALMWP-NP, cellular uptake experiments were also performed in both HT1080 cell line with high MMP expression (Figure 3) and bEnd.3 cells with negligible expression of MMP-2/9 (Figure 5) in the absence/presence of MMP specific inhibitor, metastat. The results showed that the cellular association of ALMWP-NP in HT-1080 cells was significantly reduced in the presence of the metastat. In contrast, the cellular uptake of ALMWP-NP in bEnd.3 cells was found to be significantly lower than that of LMWP-NP, but did not change in the presence of MMP inhibitor. This evidence clearly indicated that the tumor-cell-specific cellular interaction of ALMWP-NP was an MMP-dependent process, which was further confirmed by the fact that in HT-1080 cells free ALMWP competed with ALMWP-NP for the MMP-mediated cleavage and inhibited the cellular uptake of ALMWP-NP.

The application of CPP for effective cellular penetration always raises the question of its potential toxicity. Activatible CPP could be a strategy to reduce the toxicity of CPP to the nontarget cells. In this work, cytotoxicity after ALMWP-NP treatment was evaluated on bEnd.3 cells. PLA polymers are generally accepted as safe polymer matrix with good biocompatibility and biodegradability. Moreover, both PEG and PLA are materials approved by FDA.[31,32] Thus, unconjugated PEG-PLA NP was regarded as the safety control. ALMWP-NP was found to be safe as the unmodified NP, while LMWP-NP exhibited considerable cytotoxicity (Figure 6).

Pharmacokinetic study showed that Taxol exhibited the fastest systemic clearance, while all the nanoparticle formulations extended the circulation time of PTX. PTX-ALMWP-NP exhibited an overlap concentration−time curve with PTX-NP, indicating that the surface modification of ALMWP did not affect the long circulation performance of PEG. In contrast, PTX-LMWP-NP was cleared more rapidly from the circulation and obtained a significantly smaller AUC than both PTX-NP and PTX-ALMWP-NP. This could have resulted from its positive surface charge, which facilitates its rapid systemic elimination and high accumulation in the nontargeted organs such as lung and liver. On the other hand, both in vivo imaging and biodistribution data showed that ALMWP-NP exhibited a significantly increased accumulation in tumor, but not in the nontargeted tissues, suggesting that ALMWP-NP might serve as a nanocarrier with better pharmacokinetic properties for tumor-targeting drug delivery.

In vivo tumor penetration analysis showed that ALMWP-NP presented better tumor permeability than both NP and LMWP-NP (Figure 8). Although NP could reach the tumor site through the EPR effect, its low intratumor penetration made the fluorescence signal in tumor parenchyma almost invisible. In the case of LMWP-NP, due to its faster clearance and higher accumulation in the nontargeted tissues, much weaker fluorescent signals were observed in the tumor parenchyma than that of ALMWP-NP.

Thanks to the improved biodistribution profile and the enhanced tumor penetration, PTX loaded by ALMWP-NP exhibited the best antitumor efficacy. Although PTX-LMWP-NP presented stronger antiproliferation effects in vitro, which could be due to the cytotoxicity of LMWP-NP itself, PTX-ALMWP-NP showed the highest inhibition of tumor growth in vivo (Figure 11). The findings here offered robust evidence for the targeting therapeutic effects of PTX-ALMWP-NP, and might lead to a significant advancement in the application of CPPs for targeted tumor therapy.

CONCLUSION

In the present study, we constructed ALMWP, in which a polycationic LMWP segment attached to a neutralizing polyanion E10 segment via a protease-cleavable linker PLGLAG, as a novel tumor-targeting ligand to be modified onto the surface of poly(ethylene glycol)-poly(lactic acid) (PEG-PLA) nanoparticles for facilitating drug delivery with enhanced tumor targeting and penetration. The obtained ALMWP-NP exhibited significantly enhanced MMP-mediated cellular accumulation via energy-independent direct translocation, and clathrin-mediated, cytoskeleton-dependent endocytosis. Biodistribution analysis in HT-1080 tumor-bearing mice showed that ALMWP-NP significantly increased the accumulation of PTX in the tumor site but not the nontarget tissues, while LMWP-NP was rapidly eliminated and highly accumulated in the liver and spleen. ALMWP-NP also exhibited enhanced penetration into the tumor parenchyma. Thanks to the improved biodistribution profile and the enhanced tumor penetration, PTX-ALMWP-NP exhibited improved antitumor efficacy over both PTX-NP and PTX-LMWP-NP. The findings together suggested that ALMWP-NP could be used as an effective tumor-targeting drug delivery system.

AUTHOR INFORMATION

Corresponding Author

*J. Chen: Tel. +86-21-51980066; fax +86 21 51980069; e-mail: chenjun@fudan.edu.cn. X. Gao: Tel./fax +86-21-63846590-776451; e-mail: shellygao1@yahoo.com.cn.

Author Contributions

The first two authors contributed equally to this work.

Notes

The authors declare no competing financial interest.

ACKNOWLEDGMENTS

This work was supported by National Key Basic Research Program (2010CB529800), National Natural Science Foundation of China (81072592), National Science and Technology major Project (2012ZX09304004), Program for New Century Excellent Talents in University, Grants from Shanghai Science and Technology Committee (11430702200, 12ZR1416300 and 12nm0502000), Innovation Program of Shanghai Municipal Education Commission (12ZZ107) and SJTU Funding (AE4160003).

REFERENCES

(1) Bae, Y. H., and Park, K. (2011) Targeted drug delivery to tumors: myths, reality and possibility. *J. Controlled Release 153*, 198−205.

(2) Maeda, H. (2010) Tumor-selective delivery of macromolecular drugs via the EPR effect: background and future prospects. *Bioconjugate Chem. 21*, 797−802.

(3) Kuil, J., Velders, A. H., and van Leeuwen, F. W. (2010) Multimodal tumor-targeting peptides functionalized with both a radio- and a fluorescent label. *Bioconjugate Chem. 21*, 1709−1719.

(4) Muro, S. (2012) Challenges in design and characterization of ligand-targeted drug delivery systems. *J. Controlled Release 164*, 125−137.

(5) Kwon, I. K., Lee, S. C., Han, B., and Park, K. (2012) Analysis on the current status of targeted drug delivery to tumors. *J. Controlled Release 164*, 108−114.

(6) Nori, A., Jensen, K. D., Tijerina, M., Kopeckova, P., and Kopecek, J. (2003) Tat-conjugated synthetic macromolecules facilitate cytoplasmic drug delivery to human ovarian carcinoma cells. *Bioconjugate Chem. 14*, 44−50.

(7) Ifediba, M. A., Medarova, Z., Ng, S. W., Yang, J., and Moore, A. (2010) siRNA delivery to CNS cells using a membrane translocation peptide. *Bioconjugate Chem. 21*, 803−806.

(8) Bendifallah, N., Rasmussen, F. W., Zachar, V., Ebbesen, P., Nielsen, P. E., and Koppelhus, U. (2006) Evaluation of cell-penetrating peptides (CPPs) as vehicles for intracellular delivery of antisense peptide nucleic acid (PNA). *Bioconjugate Chem. 17*, 750−758.

(9) Saalik, P., Elmquist, A., Hansen, M., Padari, K., Saar, K., Viht, K., Langel, U., and Pooga, M. (2004) Protein cargo delivery properties of cell-penetrating peptides. A comparative study. *Bioconjugate Chem. 15*, 1246−1253.

(10) Tsui, B., Singh, V. K., Liang, J. F., and Yang, V. C. (2001) Reduced reactivity towards anti-protamine antibodies of a low molecular weight protamine analogue. *Thromb. Res. 101*, 417−420.

(11) Liang, J. F., Zhen, L., Chang, L. C., and Yang, V. C. (2003) A less toxic heparin antagonist–low molecular weight protamine. *Biochemistry (Moscow) 68*, 116−120.

(12) Lee, L. M., Chang, L. C., Wrobleski, S., Wakefield, T. W., and Yang, V. C. (2001) Low molecular weight protamine as nontoxic heparin/low molecular weight heparin antidote (III): preliminary in vivo evaluation of efficacy and toxicity using a canine model. *AAPS Pharmsci. 3*, E19.

(13) Teesalu, T., Sugahara, K. N., Kotamraju, V. R., and Ruoslahti, E. (2009) C-end rule peptides mediate neuropilin-1-dependent cell, vascular, and tissue penetration. *Proc. Natl. Acad. Sci. U. S. A. 106*, 16157−16162.

(14) Olson, E. S., Aguilera, T. A., Jiang, T., Ellies, L. G., Nguyen, Q. T., Wong, E. H., Gross, L. A., and Tsien, R. Y. (2009) In vivo characterization of activatable cell penetrating peptides for targeting protease activity in cancer. *Integr. Biol. (Camb.) 1*, 382−393.

(15) Curran, S., and Murray, G. I. (1999) Matrix metalloproteinases in tumour invasion and metastasis. *J. Pathol. 189*, 300−308.

(16) Erster, O., Thomas, J. M., Hamzah, J., Jabaiah, A. M., Getz, J. A., Schoep, T. D., Hall, S. S., Ruoslahti, E., and Daugherty, P. S. (2012) Site-specific targeting of antibody activity in vivo mediated by disease-associated proteases. *J. Controlled Release 161*, 804−812.

(17) Gao, X., Wu, B., Zhang, Q., Chen, J., Zhu, J., Zhang, W., Rong, Z., Chen, H., and Jiang, X. (2007) Brain delivery of vasoactive intestinal peptide enhanced with the nanoparticles conjugated with wheat germ agglutinin following intranasal administration. *J. Controlled Release 121*, 156−167.

(18) Zeng, N., Hu, Q., Liu, Z., Gao, X., Hu, R., Song, Q., Gu, G., Xia, H., Yao, L., Pang, Z., Jiang, X., Chen, J., and Fang, L. (2012) Preparation and characterization of paclitaxel-loaded DSPE-PEG-liquid crystalline nanoparticles (LCNPs) for improved bioavailability. *Int. J. Pharm. 424*, 58−66.

(19) Jiang, T., Olson, E. S., Nguyen, Q. T., Roy, M., Jennings, P. A., and Tsien, R. Y. (2004) Tumor imaging by means of proteolytic activation of cell-penetrating peptides. *Proc. Natl. Acad. Sci. U. S. A. 101*, 17867−17872.

(20) Weissleder, R., and Mahmood, U. (2001) Molecular imaging. *Radiology 219*, 316−333.

(21) Hu, K., Li, J., Shen, Y., Lu, W., Gao, X., Zhang, Q., and Jiang, X. (2009) Lactoferrin-conjugated PEG-PLA nanoparticles with improved brain delivery: in vitro and in vivo evaluations. *J. Controlled Release 134*, 55−61.

(22) Xia, H., Gao, X., Gu, G., Liu, Z., Zeng, N., Hu, Q., Song, Q., Yao, L., Pang, Z., Jiang, X., Chen, J., and Chen, H. (2011) Low molecular weight protamine-functionalized nanoparticles for drug delivery to the brain after intranasal administration. *Biomaterials 32*, 9888−9898.

(23) Scott, A. J., and Woods, J. P. (2000) Monitoring internalization of Histoplasma capsulatum by mammalian cell lines using a fluorometric microplate assay. *Med. Mycol. 38*, 15−22.

(24) Coussens, L. M., Fingleton, B., and Matrisian, L. M. (2002) Matrix metalloproteinase inhibitors and cancer: trials and tribulations. *Science 295*, 2387−2392.

(25) Guo, J., Gao, X., Su, L., Xia, H., Gu, G., Pang, Z., Jiang, X., Yao, L., Chen, J., and Chen, H. (2011) Aptamer-functionalized PEG-PLGA

nanoparticles for enhanced anti-glioma drug delivery. *Biomaterials 32*, 8010−8020.
(26) Chen, J., Liu, T. W., Lo, P. C., Wilson, B. C., and Zheng, G. (2009) "Zipper" molecular beacons: a generalized strategy to optimize the performance of activatable protease probes. *Bioconjugate Chem. 20*, 1836−1842.
(27) Liu, T. W., Chen, J., and Zheng, G. (2011) Peptide-based molecular beacons for cancer imaging and therapy. *Amino Acids 41*, 1123−1134.
(28) Lovell, J. F., Liu, T. W., Chen, J., and Zheng, G. (2010) Activatable photosensitizers for imaging and therapy. *Chem. Rev. 110*, 2839−2857.
(29) Liu, T. W., Akens, M. K., Chen, J., Wise-Milestone, L., Wilson, B. C., and Zheng, G. (2011) Imaging of specific activation of photodynamic molecular beacons in breast cancer vertebral metastases. *Bioconjugate Chem. 22*, 1021−1030.
(30) Liu, D., Mori, A., and Huang, L. (1992) Role of liposome size and RES blockade in controlling biodistribution and tumor uptake of GM1-containing liposomes. *Biochim. Biophys. Acta 1104*, 95−101.
(31) Langer, R. (1997) Tissue engineering: a new field and its challenges. *Pharm. Res. 14*, 840−841.
(32) Adams, M. L., Lavasanifar, A., and Kwon, G. S. (2003) Amphiphilic block copolymers for drug delivery. *J. Pharm. Sci. 92*, 1343−1355.